POSEIDON: PORTABLE OCULAR SURFACE EVALUATION WITH INTEGRATED DESIGN OF HARDWARE AND NETWORK

Juntao Qiu[1,], Yaping Zhao[1,*,†], Yuxing Li[1], Allie Lee[2], Vincent Tam[1], Edmund Y. Lam[1,†]*

[1]*Department of Electrical and Electronic Engineering, The University of Hong Kong, Hong Kong, China*
[2]*Department of Ophthalmology, The University of Hong Kong, Hong Kong, China*
[*]Equal contribution [†]Corresponding authors

2026 IEEE 23rd International Symposium on Biomedical Imaging (ISBI) | 979-8-3315-7763-6/26/$31.00 ©2026 IEEE | DOI: 10.1109/ISBI61048.2026.11515330

ABSTRACT

This work presents **POSEIDON**, a portable ocular surface evaluation system built on a hardware–software co-design paradigm for real-time, quantitative assessment of ocular surface diseases. The system integrates dual-modality imaging into an end-to-end pipeline, with a lightweight network for meibomian gland delineation on edge devices with limited power and memory. By unifying imaging, computation, and clinical interpretation in a compact system, POSEIDON establishes a scalable route toward intelligent ocular surface disease analysis and democratized eye-health monitoring.

***Index Terms*—** biomedical imaging, ocular surface disease, meibomian gland dysfunction, infrared meibography

1. INTRODUCTION

Ocular surface diseases (OSDs) encompass chronic disorders of the cornea, conjunctiva, and eyelids, with prevalence rising due to environmental and lifestyle factors [1]. Among these, dry eye disease (DED) is the most prevalent, with a global prevalence of 7%–52% [2]. Meibomian gland dysfunction (MGD), the primary pathogenic driver, underlies 80%–90% of DED cases [3]. Progressive gland dropout and atrophy reduce lipid secretion and destabilize the tear film, therefore objective meibomian gland (MG) morphology assessment for early detection and clinical management is necessary [4].

Despite this need, evaluation remains largely qualitative. IR meibography is commonly graded by visual inspection, which suffers from observer variability [5]. Manual segmentation can improve accuracy but requires 12–25 minutes per image [6], making it impractical for large-scale use.

Early automation relied on handcrafted pipelines such as thresholding, morphological filters, and texture descriptors [7], which were vulnerable to illumination changes and imaging artifacts. Curve-fitting models helped characterize eyelid margins but still required manual ROI selection [8]. With the advent of deep learning, CNN-based frameworks have been applied to MG segmentation and severity grading. Examples include U-Net pipelines extracting gland morphology [9], generative models addressing reflection artifacts [6], and semantic segmentation networks quantifying atrophic regions [10, 11]. While effective, these models are often computationally intensive, trained on limited datasets, and confined to clinic-based systems.

Lightweight architectures are well established in RGB imaging, particularly with YOLO-based detectors [12], but efficient solutions for IR meibography remain limited. Additional hardware and data-flow complexity in IR imaging lead to issues of algorithmic efficiency. Meanwhile, portable devices such as MeiboVue and Ezer Sapphire support high-resolution acquisition but lack embedded analytics [13], creating a gap between imaging and actionable insights.

To address these, we propose a hardware–software co-designed system for automated MG segmentation and MGD assessment. The framework enables real-time, on-device inference across both IR and RGB modalities, demonstrating point-of-care viability. The main contributions are:

- Design of a hardware–software integrated system for real-time segmentation and diagnostics on edge devices.
- Dual-modality pipeline integrating imaging with lightweight neural networks tailored for low-resource deployment.
- Prototype validation on public and clinical datasets, showing both segmentation accuracy and system feasibility.

2. SYSTEM OVERVIEW

The proposed system integrates RGB anterior eye imaging and infrared (IR) meibography within a dual-modality pipeline to enable comprehensive ocular surface evaluation. As Fig. 1 shows, the workflow comprises five steps: imaging, preprocessing, segmentation, indexing, and reporting.

During acquisition, complementary modules operate: the RGB module captures anterior segment photos for general ocular surface screening (e.g., pain, injury, blurred vision), while the IR one acquires high-resolution meibography of upper/lower eyelids to characterize MG morphology—including gland area, Meiboscore, and structural irregularities.

This work is supported in part by the Innovation and Technology Fund (ITS/341/23) of Hong Kong, China.

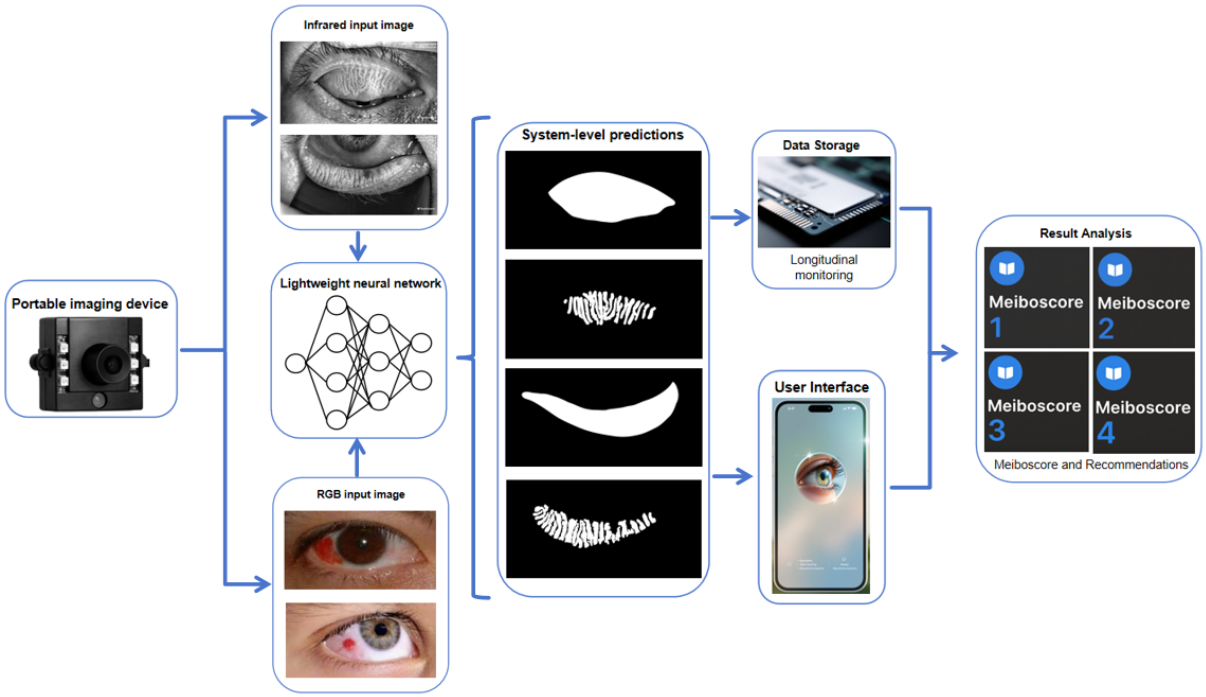

Fig. 1: Dual-modality system overview with RGB anterior eye imaging and IR meibography.

Captured images undergo standardized preprocessing. For IR data, this includes eyelid region extraction and glandular mask preparation; for RGB images, vascular and conjunctival regions are enhanced to facilitate subsequent analysis. Modality-specific neural networks perform segmentation: a lightweight YOLO-based detector identifies subconjunctival hemorrhage (SCH) and conjunctivitis in RGB images, while a specially designed lightweight network segments glands in IR meibography. This hardware–software co-design enables efficient complementary analysis on low-power edge devices.

Quantitative indices are computed post-segmentation. For RGB images, SCH area proportion and vessel thickness metrics are derived, targeting vessel calibers for sensitivity to pathological dilation. For IR images, MG-to-eyelid area ratio, gland dropout counts, and irregularity patterns are quantified to generate interpretable measures aligned with clinical systems. Results are aggregated into a user-friendly interface: RGB outputs visual overlays with severity indicators, while IR outputs display MG area ratios, dropout numbers, and irregularity maps, for real-time point-of-care decision-making.

3. ALGORITHM MODULE

Since the proposed system processes multimodal data streams, an IR pathway is included for meibomian gland analysis. Unlike the RGB domain where lightweight detectors are well established, efficient algorithms tailored for IR meibography remain underdeveloped. To bridge this gap, we design a lightweight network for meibomian gland analysis in IR images [14]. The network follows a compact U-shaped architecture, and integrates task-specific mechanisms to address the major challenges of gland segmentation.

One key challenge arises when tortuous and densely packed glands appear indistinguishable at their boundaries, leading to adhesion artifacts. To alleviate this, we adopt an attention-based gating mechanism in skip connections [15]. This module filters encoder features using decoder context, thereby enhancing boundary discrimination and reducing adhesion errors for closely clustered glands. Another difficulty is incomplete or fragmented gland predictions, especially for elongated, distorted, or atrophic morphologies. To address this, the network incorporates a multi-scale representation strategy [16, 17] with residual connections and channel–spatial recalibration for enriched contextual learning and improved structural continuity.

4. EXPERIMENTS

Comparative Analysis on Public Dataset. We evaluate the efficacy of our method on the public MGD-1K benchmark [6], compared with U-Net [18], Attention-UNet [15], UNet++ [19], CPFNet [20], CS^2-Net [21], CE-Net [22], IF-Net [23], and GD-Net [24]. Five established metrics assess performance: Dice Similarity Coefficient, Intersection over Union, Sensitivity, Specificity, and Accuracy. As Fig. 2 shows, ours consistently outperforms others, providing reli-

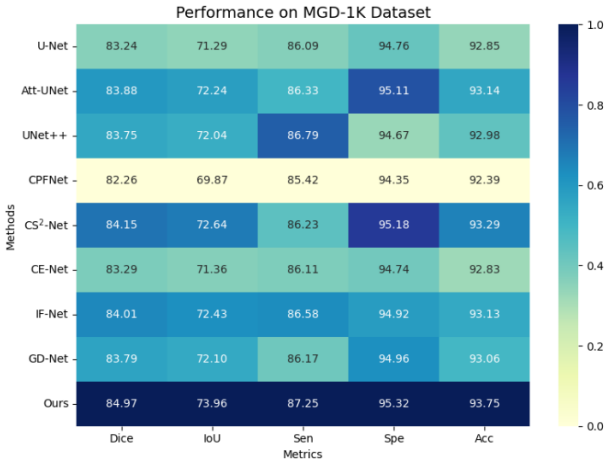

Fig. 2: MGD-1K results across five metrics.

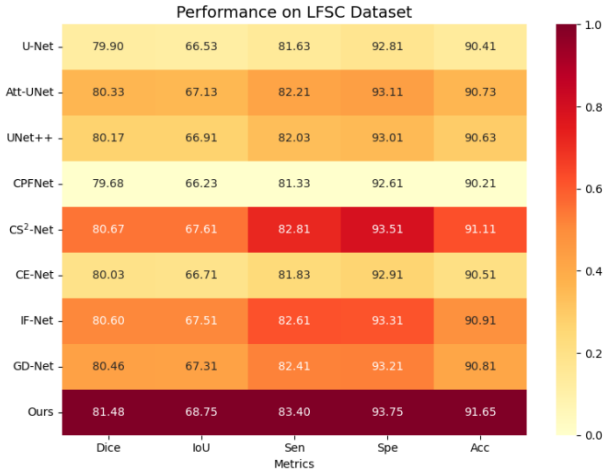

Fig. 3: LFSC clinical dataset results.

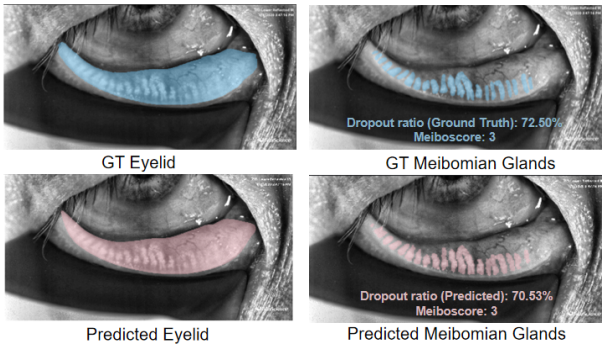

Fig. 4: Visualization of segmentation results.

able MG segmentation with accurate boundary delineation and robust preservation of gland morphology.

Cross-Dataset Validation on Clinical Data. To further assess clinical applicability, we validated the framework on the LFSC dataset [25]. As Fig. 3 shows, ours again demonstrates

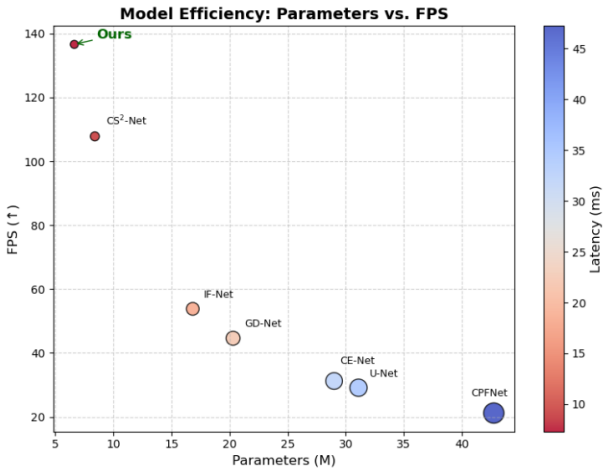

Fig. 5: Efficiency analysis.

(a) (b)

Fig. 6: Hardware system overview. (a) Portable IR meibography prototype connected to a mobile phone. (b) USB imaging module with 850 nm IR LED array for compact meibography.

superiority over existing networks across metrics. The consistent ranking across datasets highlights generalization under domain shift and supports the clinical applicability.

Visualization of Segmentation Results. As Fig. 4 shows, the predicted eyelid and gland masks align well with the ground truth, with a dropout ratio of 70.53% versus 72.50%, both corresponding to Meiboscore grade 3. This confirms reliable structural delineation and consistency with clinical indices.

Model Efficiency and Lightweight Comparison. Lightweight networks are critical for deployment in medical imaging, where memory efficiency, latency, and throughput are paramount. We implement comparisons across four key dimensions: parameter count, model size, inference speed (FPS), and latency.

As Fig. 5 shows, ours requires substantially fewer parameters and less memory, while providing faster inference.

Portable Hardware System. To facilitate practical deployment and real-world validation, we developed a compact IR meibography system (Fig. 6). The system enables the acquisition of high-contrast eyelid images. Integrated with the proposed framework, the system provides intelligent point-of-care MGD assessment, enhancing accessibility for patients with limited mobility or restricted healthcare access.

5. REFERENCES

[1] Ilene K Gipson et al., "The ocular surface: the challenge to enable and protect vision: the friedenwald lecture," *Investigative ophthalmology & visual science*, vol. 48, no. 10, pp. 4391–4398, 2007.

[2] Heiko Pult et al., "The development and evaluation of the new ocular surface disease index-6," *The Ocular Surface*, vol. 17, no. 4, pp. 817–821, 2019.

[3] Ebenezer Daniel et al., "Grading and baseline characteristics of meibomian glands in meibography images and their clinical associations in the dry eye assessment and management (dream) study," *The ocular surface*, vol. 17, no. 3, pp. 491–501, 2019.

[4] Zuhui Zhang et al., "Artificial intelligence-assisted diagnosis of ocular surface diseases," *Frontiers in Cell and Developmental Biology*, vol. 11, pp. 1133680, 2023.

[5] Heiko Pult et al., "Comparison of subjective grading and objective assessment in meibography," *Contact Lens and Anterior Eye*, vol. 36, no. 1, pp. 22–27, 2013.

[6] Ripon Kumar Saha et al., "Automated quantification of meibomian gland dropout in infrared meibography using deep learning," *The Ocular Surface*, vol. 26, pp. 283–294, 2022.

[7] Clara Llorens-Quintana et al., "Automated image processing algorithm for infrared meibography," in *Imaging Systems and Applications*, 2018, pp. IM3B–3.

[8] Clara Llorens-Quintana et al., "A novel automated approach for infrared-based assessment of meibomian gland morphology," *Translational vision science & technology*, vol. 8, no. 4, pp. 17–17, 2019.

[9] Md Asif Khan Setu et al., "Deep learning-based automatic meibomian gland segmentation and morphology assessment in infrared meibography," *Scientific reports*, vol. 11, no. 1, pp. 7649, 2021.

[10] Jiayun Wang et al., "A deep learning approach for meibomian gland atrophy evaluation in meibography images," *Translational vision science & technology*, vol. 8, no. 6, pp. 37–37, 2019.

[11] Shansi Zhang et al., "Semi-supervised semantic segmentation for light field images using disparity information," *IEEE TIP*, 2024.

[12] Peiyuan Jiang et al., "A review of yolo algorithm developments," *Procedia computer science*, vol. 199, pp. 1066–1073, 2022.

[13] Héctor Retana et al., "Development of alpha prototype of handheld device for meibography," in *Congreso Nacional de Ingeniería Biomédica*, 2022, pp. 448–458.

[14] Juntao Qiu et al., "Grace: Meibomian gland segmentation with residual attention and channel excitation," Submitted, 2025.

[15] Ozan Oktay et al., "Attention u-net: Learning where to look for the pancreas," *arXiv:1804.03999*, 2018.

[16] Yaping Zhao et al., "Efenet: Reference-based video super-resolution with enhanced flow estimation," in *CICAI*. Springer, 2021, pp. 371–383.

[17] Yaping Zhao et al., "Cross-camera deep colorization," in *CICAI*. Springer, 2022, pp. 3–17.

[18] Olaf Ronneberger et al., "U-net: Convolutional networks for biomedical image segmentation," in *MICCAI 2015*. Springer, 2015, pp. 234–241.

[19] Zongwei Zhou et al., "Unet++: A nested u-net architecture for medical image segmentation," in *DLMIA/ML-CDS (with MICCAI)*, 2018, pp. 3–11.

[20] Shuanglang Feng et al., "Cpfnet: Context pyramid fusion network for medical image segmentation," *IEEE TMI*, vol. 39, no. 10, pp. 3008–3018, 2020.

[21] Lei Mou et al., "Cs2-net: Deep learning segmentation of curvilinear structures in medical imaging," *Medical image analysis*, vol. 67, pp. 101874, 2021.

[22] Zaiwang Gu et al., "Ce-net: Context encoder network for 2d medical image segmentation," *IEEE TMI*, vol. 38, no. 10, pp. 2281–2292, 2019.

[23] Dengfeng Liu et al., "If-net: information fusion network for meibomian gland area and atrophy area segmentation," in *Medical Imaging 2023: Image Processing*. SPIE, 2023, vol. 12464, pp. 917–924.

[24] Chenpu Yao et al., "Joint segmentation of multi-class hyper-reflective foci in retinal optical coherence tomography images," *IEEE TBE*, vol. 69, no. 4, pp. 1349–1358, 2021.

[25] Yuxing Li et al., "Dual-mode imaging system for early detection and monitoring of ocular surface diseases," *IEEE TBCS*, 2024.